Temporal phosphate gradients reveal diverse acclimation responses in phytoplankton phosphate uptake

Carlos Cáceres[1,2], Sofie Spatharis[3,4], Eirini Kaiserli[5], Evangelia Smeti[6], Hugh Flowers[7], Juan A. Bonachela[1,8]

Corresponding author:

Carlos Cáceres: caceres.30@osu.edu

Juan A. Bonachela: juan.bonachela@rutgers.edu

1 Department of Mathematics and Statistics, University of Strathclyde, Livingstone Tower, 26 Richmond St, Glasgow G1 1XH, Scotland, UK.

2 Schiermeier Olentangy River Wetland Research Park, School of Environment and Natural Resources, The Ohio State University, Columbus, Ohio 43202, USA.

3 Institute of Biodiversity, Animal Health and Comparative Medicine, University of Glasgow, Glasgow, G12 8QQ, Scotland, UK.

4 School of Life Sciences, University of Glasgow, Glasgow, G12 8QQ, Scotland, UK.

5 Institute of Molecular, Cell and Systems Biology, College of Medical, Veterinary and Life Sciences, University of Glasgow, Glasgow, G12 8QQ, UK.

6 Hellenic Centre for Marine Research, Institute of Marine Biological Resources and Inland Waters, 46.7km Athens-Sounio Ave., Anavyssos, 19013, Greece.

7 Department of Chemistry, University of Glasgow, Glasgow G12 8QQ, Scotland, UK.

8 Department of Ecology, Evolution, and Natural Resources, Rutgers University, 14 College Farm Road, New Brunswick, NJ 08901 USA.

This is the accepted version of the following article: *Cáceres C, Spatharis S, Kaiserli E, Smeti E, Flowers H, Bonachela JA. Temporal phosphate gradients reveal diverse acclimation responses in phytoplankton phosphate uptake. ISME J (in press). doi 10.1038/s41396-019-0473-1.*

Abstract

Phytoplankton face environmental nutrient variations that occur in the dynamic upper layers of the ocean. Phytoplankton cells are able to rapidly acclimate to nutrient fluctuations by adjusting their nutrient uptake system and metabolism. Disentangling these acclimation responses is a critical step in bridging the gap between phytoplankton cellular physiology and community ecology. Here, we analyzed the dynamics of phosphate (P) uptake acclimation responses along different P temporal gradients by using batch cultures of the diatom *Phaeodactylum tricornutum*. We employed a multidisciplinary approach that combined nutrient uptake bioassays, transcriptomic analysis, and mathematical models. Our results indicated that cells increase their maximum nutrient uptake rate (V_{max}) both in response to P pulses and strong phosphorus limitation. The upregulation of three genes coding for different P transporters in cells experiencing low intracellular phosphorus levels supported some of the observed V_{max} variations. In addition, our mathematical model reproduced the empirical V_{max} patterns by including two types of P transporters upregulated at medium-high environmental and low intracellular phosphorus levels, respectively. Our results highlight the existence of a sequence of acclimation stages along the phosphate continuum that can be understood as a succession of acclimation responses. We provide a novel conceptual framework that can contribute to integrating and understanding the dynamics and wide diversity of acclimation responses developed by phytoplankton.

Introduction

Phytoplankton play a key role in global biogeochemical cycles, being responsible for approximately 40% of the global primary production and fueling oceanic food webs (1–3). Phytoplankton grow in the euphotic layers of aquatic environments, where concentrations of inorganic nutrients fluctuate widely. Such fluctuations affect phytoplankton community composition by favoring species and ecotypes with eco-physiological traits best suited to exploit available nutrients (4). Nutrient changes also trigger responses at the cellular level, as phytoplankton modify their eco-physiological traits, including those related to nutrient uptake (5–7). Due to the short time required for these individual level acclimation changes to occur, these responses can be relevant for exploiting a variety of conditions along the nutrient continuum, from oligotrophic environments to sharp and/or short-lived nutrient pulses (5,6,8–10). In spite of their importance, acclimation dynamics along nutrient spatiotemporal gradients are still poorly understood.

The study of phytoplankton nutrient uptake acclimation responses associated with changes in nutrient levels has been traditionally based on the variations of the maximum nutrient-uptake rate (V_{max}) and the

half saturation constant for nutrient uptake (*K*) measured from nutrient uptake bioassays (6,11,12). V_{max} and *K* are the parameters of the Michaelis-Menten equation, commonly employed to describe nutrient uptake rate as a function of the external nutrient concentration (13,14), and are linked to key eco-physiological traits (15,16): V_{max} determines the potential of the cell to take up nutrients and is related to the number of nutrient uptake sites present in the cell membrane (5,17). *K* and the ratio between V_{max} and *K* (18), indicate the efficiency of the process and define the ability of the cell to exploit oligotrophic environments (for constant V_{max}, the lower the *K* the higher the nutrient uptake). Existing literature has reported, however, contradictory relationships between V_{max} and the limiting nutrient concentration.

Most empirical studies show a higher V_{max} in cultures where nutrients are depleted, enabling the cells to improve nutrient intake abilities (6,11,12,19). In contrast to these observations, some investigations reported a higher V_{max} at high nutrient levels, suggesting that cells could take advantage of the often brief high nutrient concentrations (5,20). Regarding variations in *K*, these have been linked to the existence of different types of nutrient transporters, each of which can display different nutrient uptake rates and regulation mechanisms (20–23). Transporters have consequently been divided in high and low-affinity groups attending to their half saturation constant (23). Recent transcriptomic analyses confirmed the existence of different transporters for the same nutrient, with likely different V_{max} and *K* values and regulation mechanisms (24–28). Such transporter diversity might contribute to the aforementioned variation in V_{max} patterns.

Despite their potential relevance for the understanding of phytoplankton acclimation, there is a lack of empirical work combining V_{max} and *K* measurements with transcriptomic analysis for identifying the mechanisms underlying V_{max} and *K* variations along the nutrient spatiotemporal gradient. Furthermore, most V_{max} studies have been addressed using steady state cultures, i.e. chemostats, or batch cultures sampled at unique time shots (but see ref. 17), which has limited the comprehension of the dynamics of the acclimation process and the development of mechanistic mathematical models. Indeed, no existing theoretical framework integrates the wide diversity of acclimation patterns occurring along the spatiotemporal nutrient gradient. Theories considering acclimation responses typically focus on the negative relationship between V_{max} and nutrient concentrations, mostly using phenomenological expressions (7,15,29).

Here, we aimed to fill this gap by i) understanding mechanistically the dynamics of phytoplankton phosphate uptake acclimation along temporal gradients of phosphate (hereafter P), and ii) providing a theoretical framework able to integrate the wide diversity of nutrient uptake acclimation responses and

consider the temporal dimension of the acclimation process. To this end, we followed a multidisciplinary approach combining P uptake bioassays, transcriptomic analysis, and mathematical models (30). We monitored for the first time the dynamics (i.e. behavior through several consecutive time points) of V_{max} and K for phosphate along different P gradients by using batch cultures of the diatom *Phaeodactylum tricornutum* supplied with different pulses of P. We also measured the expression of genes coding for P transporters and proteins involved in phosphorus metabolism. Finally, we developed a mechanistic model that integrates the specific temporal patterns of acclimation observed in our experiments in a continuous moving picture (30). Building on previous work (31), we considered two kinds of nutrient transporters operating in parallel (32). The combination of our empirical and theoretical results revealed a sequence of acclimation responses along the temporal nutrient gradients that includes both positive and negative V_{max}-nutrient relationships. Our results provide a novel ecological framework that can contribute to understanding and constraining the dynamics and wide diversity of nutrient uptake acclimation responses displayed by phytoplankton.

Material and methods

Phytoplankton cultures and experimental design

Strain 1052/1A (isolated off Plymouth, UK) of the diatom *P. tricornutum* was obtained from the culture collection of the Scottish Association of Marine Sciences (SAMS). *P. tricornutum* is an emerging model species in molecular biology. It mainly grows in coastal waters from tropical and temperate latitudes, including estuaries and areas affected by tidal mixing. Some of these environments show strong and sharp nutrient variations (33–35). This makes *P. tricornutum* a good candidate for the present study. We inoculated 10 flasks with 5 x 10^4 cells mL^{-1} and F/2 medium (200 mL) with a reduced concentration of P (3 µM instead of the 36.2 µM from F/2) to ensure phosphorus limitation. Based on Zhang et al. (8), we also added a mix of antibiotics containing penicillin (1.00 gL^{-1}), kanamycin (0.50 gL^{-1}), and neomycin (0.25 gL^{-1}) to prevent the growth of bacteria. We used a light intensity of 20 µmol m^{-2} s^{-1}. Temperature was set at 20°C and shaking at 140 rpm.

Five days after starting the cultures, we collected different aliquots from one of the ten flasks (see Fig. S1 for a schematic diagram of the experimental design). These aliquots were employed for measuring V_{max}, K, intracellular phosphorus content (*i.e.* quota, Q), and expression of genes related to phosphorus metabolism (see below). One day later (day 6), when cells were in a transition to a stationary phase (*i.e.* phosphorus limited but not totally starved; Fig. S2), we added nutrient pulses (F/2 medium with different

levels of P) to the nine remaining flasks: three flasks were supplied with no P (reference treatment, P_{ref}), three with 3 µM P (low P pulse treatment, P_{low}), and three with 15 µM P (high P pulse treatment, P_{high}). One flask from each treatment was sampled and measurements performed 3.5 h, 28 h and 100 h after adding the corresponding pulse of nutrients, so that we obtained a time series for the three different P addition levels (Fig. S1). The whole experiment was carried out three times with one week in between to generate three replicates (Fig. S1). In order to keep the metabolic state of the cells as similar as possible among the three replicates, the cells inoculated to each experiment came from cultures sequentially initiated (also with one week in between). We alternated the time at which each P pulse was added among experimental replicates to prevent a spurious association between P pulse and uptake traits due to the effect of the cell dial cycle. For similar reasons, we used continuous (i.e. 24 h) illumination.

Phosphate uptake bioassays

We estimated V_{max} and effective K (K_{eff}) by performing P uptake bioassays based on Lomas et al. (10). We incubated solutions (10 mL) containing 7,500 cells mL^{-1}, 0.20 µCi of $H_3{}^{33}PO_4$, and different amounts of non-radioactive H_3PO_4 (from 0.1 to 7 µM) for 20 minutes, so that each solution contained a different concentration of non-radioactive H_3PO_4 (see SI for further details). Samples were filtered and the radioactivity in the filters was measured using a scintillation counter. The rate of P uptake rate (V, fmol $cell^{-1}$ d^{-1}) was then estimated from the measured radioactivity and the P concentration during incubations (Eq. [S2]). We fitted the Michaelis-Menten function (Eq. [S1]) to P uptake observations using R software to obtain the curve (Fig. S3) and its associated parameters, V_{max} and K_{eff}. We repeated this process with the different cultures (*i.e.* flasks) to estimate V_{max} and K_{eff} in each P pulse treatment 24 h before and 3.5 h, 28 h and 100 h after P pulses (Fig. S1).

Intracellular phosphorus measurement

The culture aliquots (25 mL) were filtered through a 47 mm pre-combusted glass fiber filter with 1.2 µm of pore size. The filters were then washed with salt water and an oxalate solution to remove any P adsorbed to the cells (36). Subsequently, we digested the organic phosphorus in the filters by using concentrated nitric acid (see SI). Filters washed with salt water and oxalate solution were used as a negative control (blank). The phosphorus quota (fmol $cell^{-1}$) was estimated from the P concentration in the digested solution (Eq. [S3]), which was measured using a flow injection autoanalyzer.

Gene expression analysis: RNA extraction and quantitative Real-Time PCR analysis (qRT-PCR)

RNA extraction was performed on a 150 mL cell culture aliquot that was centrifuged at 4,000 g for 15min. The supernatant was removed and the cells (pellet) were stored in -80 C. Total RNA was extracted using the RNAeasy plant mini kit (Qiagen) and cDNA was synthesized from 250 ng of RNA using the QuantiTect reverse transcription kit (Qiagen). Quantitative RT-PCR was performed to analyze the expression of the following genes: *HISTONE 4* (*H4*) (ref. 37), Na/P co-transporters 47666 (*Na/Pi 47666*) and 47667 (*Na/Pi 47667*), P transporter 39515 (*Pi 39515*), Alkaline phosphatase 49678 (*AP 49678*), and Carbamoyl phosphate synthetase 1583 (*CPS 1583*) (ref. 28; see SI for further details). Normalization of the quantitative real-time PCR data was calculated by geometric averaging of the internal reference gene *H4* (refs. 38,39).

Statistical analyses

Uptake traits, quota and cell abundance

The effect of P pulses (P_{ref}, P_{low}, and P_{high}) on the temporal dynamics of V_{max}, K_{eff}, V_{max}:K_{eff}, Q, and N was tested with analysis of variance (ANOVA) on a linear mixed effects model including P pulse and time as fixed factors and experiment as a random factor (each experiment constitutes a separate set of measurements; see SI for a detailed description of the model). Data were fourth-root transformed to approximate to homoscedasticity and normality assumptions (Fig. S4; ref. 40). The occurrence of differences in the response variables among the three P temporal gradients corresponding to the three nutrient pulses would be reflected by a significant effect of the factor *P Pulse* or an interaction between the factors *P pulse* and *Time*. Models were fitted by employing the *nlme* R package (41,42). To test for statistical differences between specific levels of fixed factors, we conducted pairwise comparisons using the *emmeans* R package (43) and correcting p-values according to the Benjamini and Hochberg (44) procedure (see SI for further details).

Gene expression

The relative expression of each gene (%) was estimated by using P_{ref} 3.5 h after the pulse as a reference. Since we were only able to extract RNA from 2 experiments, we focused on whether the response presented the same trend across different P pulses and time points.

Mathematical model for phosphate uptake acclimation

Our mechanistic eco-physiological model describing acclimation responses uses a modified Droop model (14) to represent the link between the specific growth rate (μ, d^{-1}) and the intracellular content or quota (fmol $cell^{-1}$) of the limiting nutrient, in our case phosphorus:

$$\mu(Q,N) = \mu_\infty \left(1 - \frac{Q_{\min}}{Q}\right) - \alpha N^2, \qquad [1]$$

where μ_∞ is the growth rate for infinite Q, Q_{min} is the minimum quota required for growth (*i.e.* Q when μ = 0), and N is the abundance of cells (cells L^{-1}). Differently from the usual Droop equation, we included a αN^2 term representing generically density-dependent effects such as mutual shading or the release of secondary metabolites to the medium that may occur, ultimately impacting growth at the cellular level (45,46; see SI for further details). The temporal dynamics of the population abundance are given by:

$$\frac{dN}{dt} = \mu(Q,N)\, N, \qquad [2]$$

where we have considered any source of mortality negligible. The change with time of Q, in turn, depends on the balance between phosphate uptake rate (V) and cell division (note that cell division leads to a distribution of the cell's phosphorus content):

$$\frac{dQ}{dt} = V - \mu(Q,N)\, Q\,. \qquad [3]$$

V (fmol $cell^{-1}$ d^{-1}) is represented as a function of the external P concentration (µmol L^{-1}) by using a modified version of the Michaelis-Menten´s equation that considers the potential effect that the simultaneous operation of several types of transporters may have on the uptake of the focal nutrient. Thus, V is estimated by adding the uptake associated with all transporter types for P (32):

$$V = \sum_{i=1}^{j} V_{\max,i}\, \frac{P}{P + K_{\text{eff},i}}\,, \qquad [4]$$

where j is the number of different transporter types, and $V_{max,i}$ and $K_{eff,i}$ are the maximum uptake rate and effective half saturation constant linked to transporter type i (see SI).

We considered two types of P transporters (j = 2): $transporter_1$ and $transporter_2$, which represent high-affinity (low K) and low-affinity (high K) transporters, respectively (see SI and ref. 23). The effective V_{max}

measured in the uptake bioassays effectively includes the transporter-specific $V_{max,i}$, in turn linked to the abundance (per cell) of each type of transporter *i* (n_i) (see SI for further details).

Because the focal acclimation response here is the cell´s ability to regulate the number transporters of each type as nutrient availability changes, we represented explicitly the dynamics of the abundance of each type of transporter as a balance between the synthesis and decrease in number due to cell division. Based on Lomas et al. (10), transporter$_1$ is upregulated at low intracellular P levels, which facilitates survival in oligotrophic environments:

$$\frac{dn_1(t)}{dt} = v_1\, H\left(c_H - \sum_{i=1}^{j} A_{rel,i}\,(t)\right) F\left(\frac{c_{F,a}Q_{\min} - Q(t)}{c_{F,a}Q_{\min} - Q_{\min}}\right) - n_1(t)\,\mu(Q,N)\,, \qquad [5]$$

where v_1 is the maximum synthesis rate of transporter$_1$ (transporters d^{-1}). *F* is a sigmoid function representing the expression of transporter:

$$F\left(\frac{c_{F,a}Q_{\min} - Q(t)}{c_{F,a}Q_{\min} - Q_{\min}}\right) = \frac{1}{1 + e^{-c_{F,b}\left(\frac{c_{F,a}Q_{\min} - Q(t)}{c_{F,a}Q_{\min} - Q_{\min}}\right)}}\,, \qquad [6]$$

The expression of transporter$_1$ is maximum when $Q = Q_{min}$ and minimum when $Q >> Q_{min}$. Note that we replaced the maximum quota (Q_{max}) from the Lomas et al. (10) function with $c_{F,a}\,Q_{min} \leq Q_{max}$, which effectively allowed us to calibrate with our experimental data the value of *Q* at which high-affinity transporters become upregulated. This modification of the *F* function implied that, as in the case of the growth rate, the gene expression variations of high-affinity transporters mainly occurred at low *Q* values. Both $c_{F,a}$ and $c_{F,b}$ control the shape of the function. Finally, *H* is a Heaviside function that limits the synthesis of transporters when the proportion of the cell surface occupied by transporters (A_{rel}) surpasses a certain threshold (c_H): $H = 0$ if $\sum_{i=1}^{j} A_{rel,i}\,(t) > c_H$, or $H = 1$ if $\sum_{i=1}^{j} A_{rel,i}\,(t) < c_H$, where $\sum_{i=1}^{j} A_{rel,i}\,(t) = \sum_{i=1}^{j} n_i\,(t)\,\frac{r_{s,i}^2}{r_c^2}$). Thus, high and low affinity transporters compete for the cell surface (see SI for further details).

On the other hand, transporter$_2$ is upregulated at high environmental P levels, enabling the cell to take advantage of P pulses:

$$\frac{dn_2(t)}{dt} = v_2\, H\left(c_H - \sum_{i=1}^{j} A_{rel,i}\,(t)\right) H\left(\frac{V_2(t)}{V_{\max,2}(t)} - g_H\right) - n_2(t)\,\mu(Q,N)\,, \qquad [7]$$

where v_2 is the maximum synthesis rate of transporter$_2$. We represent the expression of transporter$_2$ as a switch, using a Heaviside function that stops the synthesis of transporters when the ratio $V_2/V_{max,2}$, the fraction of occupied transporters (31), falls below a threshold g_H (see SI for further details). This formulation implies that transporter$_2$ has both transporter and signaling functions and is therefore considered a transceptor (47). We assumed that both type of transporters can operate simultaneously. Nonetheless, the model could be modified to take into account the potential occurrence of feedback mechanisms preventing the simultaneous operation of high and low affinity transporters (47).

Finally, the temporal dynamics of the P concentration in the medium, affected by the pulse of P when t = 6 days, is provided by:

$$\frac{dP}{dt} = -V(t)\,N(t)\,, \qquad [8]$$

The specific values assigned to each parameter and the initial conditions were based on the experimental results and design (see SI text and Table S1). Simulations including only transporter$_1$ or transorter$_2$ were also run to compare the V_{max} predictions with those obtained when both transporters were considered.

Results

Observed dynamics of uptake traits

Phosphorus limited cultures of *P. tricronutum* were supplied with different levels of P pulses (0, 3, and 15 µM P; named P_{ref}, P_{low}, and P_{high}, respectively). Measuring phosphate uptake traits at three time points following P pulses enabled us to track the dynamics of the acclimation process. The temporal behaviour of V_{max}, obtained from P uptake curves, differed depending on the pulse of P (Fig. 1a). This was confirmed by the significant interaction between *P pulse* and *Time* (ANOVA, $p < 0.01$; Table S2). V_{max} in P_{ref} was similar along the whole experiment (pairwise contrasts, $p > 0.10$; Table S3). On the contrary, V_{max} showed a V-shape pattern in P_{low} and a sharp decrease without a subsequent recover in P_{high} (Fig. 1a). Specifically, V_{max} was higher in P_{high} than in P_{ref} 3.5 h after the nutrient pulse (pairwise contrast, $p < 0.05$). However, V_{max} notably decreased between 3.5 h and 28 h after the pulse of nutrients in P_{low} and, more markedly, in P_{high} (pairwise contrasts, $p < 0.01$). One hundred hours after the nutrient pulse, V_{max} in P_{low} recovered the baseline levels observed in P_{ref} (pairwise contrast, $p > 0.30$) but remained low in P_{high} (pairwise contrast, $p < 0.01$).

This is the accepted version of the following article: *Cáceres C, Spatharis S, Kaiserli E, Smeti E, Flowers H, Bonachela JA. Temporal phosphate gradients reveal diverse acclimation responses in phytoplankton phosphate uptake. ISME J (in press). doi 10.1038/s41396-019-0473-1.*

The dynamics of K_{eff} are shown in Fig. 1b. We did not observe a significant effect of *P pulse* on K_{eff} (ANOVA, $p > 0.14$; Table S2), but we found a marginally significant effect of *P pulse* 3.5h after the nutrient pulses (ANOVA, $n = 9$, $p < 0.10$). As a result of the effect of *P pulse* on the dynamics of V_{max}, the V_{max}:K_{eff} ratio temporal behavior was also affected (Fig. S5; Table S2).

The addition of P also affected the dynamics of intracellular phosphorus quota (Fig. 1c). We found a significant interaction between *P pulse* and *Time* (ANOVA, $p < 0.05$; Table S2). 3.5h after the nutrient pulse Q was higher in P_{high} than in P_{ref} (Fig. 1c; pairwise contrast, $p < 0.01$; Table S3). Differences in Q among P pulse treatments decreased with time and were related to changes in V_{max} (Figs. 1c and S6). Finally, the P pulses also altered population growth, as revealed by the significant effect of *P pulse* on population abundances (Fig. 1d; ANOVA, $p < 0.01$; Table S2). One hundred hours after the nutrient pulse, cell concentrations were higher in P_{high} than in P_{ref} (Fig.1d; pairwise contrast, $p < 0.05$; Table S3). This higher growth in P_{high} contributed to the marked quota decrease observed from 3.5 h to 100 h (Fig. 1c).

Modelled dynamics of uptake traits

The temporal behavior of V_{max} predicted by our model with two types of nutrient transporters and different regulation mechanisms matched the patterns observed empirically. The magnitude of the P pulses affected the *in silico* V_{max} dynamics (Fig. 2a). The upregulation of transporter$_2$ led to a peak in the simulated V_{max} just after the pulse of P in both P_{low} and P_{high} (Fig. 2c). The V_{max} peak in P_{high} was higher than in P_{low} because the environmental P concentrations remained for a longer time period above the threshold level (g_H) that keeps low-affinity transporter upregulated (Figs. 2c, f). A high growth rate (Fig. 2g), which reduced the amount of transporters per cell, and the downregulation of high and low-affinity transporters lead to a subsequent V_{max} decrease (Fig. 2b, c). Both the high growth rate and the downregulation of high-affinity transporters were promoted by the high phosphorus quota (Fig. 2e; Eq. [6]), whereas the downregulation of low-affinity transporters was caused by the low environmental P levels (Fig. 2f; Eq. [7]). This V_{max} decrease did not occur in P_{ref}, where Q was close to Q_{min} and $V_{max,1}$ rose up to the threshold set by the maximum cell surface area occupied by P transporters, being the system close to a stationary phase by the end of the simulation (Fig. 2; Eq. [5]).

The decrease in V_{max} in P_{low} transitioned to an increase within the first 24 h after the P pulse. This V_{max} recovery was promoted by the upregulation of transporter$_1$ as a consequence of the reduction of Q, and stopped a few hours later when $V_{max,1}$ reached the limit set by the maximum cell surface area occupied by uptake sites (Fig. 2a, b, e; Eq. [6]). On the other hand, the long-lasting V_{max} and $V_{max,1}$ decreases in P_{high}

ceased at late stages of the simulation as cell depleted P reserves. Interestingly, the simulations carried out using a version of our model with just transporter$_1$ or transporter$_2$ were not able to qualitative reproduce all the V_{max} patterns: a model including only transporter$_1$ did not capture the rise in V_{max} just after P pulses (Fig.S7a), whereas a model with only transporter$_2$ failed to reproduce the recovering in V_{max} observed in P_{low} 100h after P pulse (Fig.S7b).

The K_{eff} peaks observed in P_{low} and P_{high} after the pulse of P (Fig. 2d) were fostered by the upregulation of low-affinity transporters, which show a high K, and the increases in diffusion limitation ultimately caused by V_{max} raises (see Eq. [S5]). The subsequent K_{eff} decrease and rebound found in both P_{low} and P_{high} is explained by variations in diffusion limitation, ultimately resulting from variations in V_{max} (Fig. 2a, d; see Eq. [S5]). As a result of the effects of the pulses of P on V_{max} and K_{eff} the temporal dynamics of the V_{max}:K_{eff} ratio were also affected (Fig. S8).

Gene expression

In our experiments, all the genes analyzed related to phosphorus metabolism (*AP 49678*, *CPS 1583*), including the three genes coding for P transporters (*Na/Pi 47666, Na/Pi 47667, Pi 39515*), were downregulated in both P_{low} and P_{high} just after the P pulse (Figs. 3 and S9). The stronger gene downregulation in P_{high} was associated with a higher phosphorus quota, which supports the role assigned to the intracellular P content in the regulation of transporter$_1$ (see F function in methods). Indeed, the decrease in the expression of *Na/Pi 47666*, *Na/Pi 47667*, and *Pi 39515* transporters within the first 28 h supports the reduction of V_{max} empirically observed and $V_{max,1}$ predicted by our model (Figs. 1a and 2b). Furthermore, the expression of these transporters in P_{ref} showed a similar temporal behaviour to that reported for V_{max} and $V_{max,1}$. The downregulation of P transporters in P_{low} and P_{high} ceased 100 h after P pulses, when the three P added treatments showed similar expression values (Fig. 3a-c).

Discussion

We addressed the dynamics of phosphate uptake traits in different P temporal gradients resulting from pulses of different magnitudes. Our results revealed two opposite V_{max}-nutrient trends along the nutrient temporal gradient: in both P_{high} and P_{low} we observed an increase in V_{max} just after the P pulse, followed by a decrease observed 28 h after the P pulse. In the case of P_{low}, V_{max} eventually recovered the values observed before the pulse. These changes in V_{max} were accompanied by changes in Q, and the expression of genes involved in P uptake and metabolism. Variations in V_{max} associated with different nutrient conditions have been previously described and modelled, especially those V_{max} increases occurring under

oligotrophic conditions (6,7,10,29). However, to the best of our knowledge, none of these previous studies reported different V_{max}-nutrient patterns along a nutrient continuum and the transition of V_{max} between opposite trends, nor provided a mechanistic theoretical framework broad enough to integrate the observed diversity of phytoplankton nutrient uptake acclimation responses.

The key feature that allows our mathematical model to reproduce the empirical V_{max} dynamics is the inclusion of two types of P transporters with different regulation mechanisms: the synthesis of transporter$_1$ (high-affinity) and transporter$_2$ (low-affinity) depended on intracellular phosphorus quota and $V_2/V_{max,2}$, respectively. The regulation proposed for transporter$_1$ was supported empirically by the upregulation at low phosphorus levels of the three genes coding for P transporters (Fig. 3), and has been widely reported for high-affinity transporters (17,23,25,48). On the other hand, none of the genes analyzed showed a regulation similar to transporter$_2$. The regulation of transporters right after P pulses in phosphorus-limited phytoplankton cultures has been less analyzed. Nonetheless, Feng et al. (49), in a proteomic analysis in *P. tricornutum* observed higher levels of a permease involved in P uptake in phosphorus-replete than in phosphorus-limited conditions. Moreover, a higher activity of low-affinity transporters at high P concentrations, regulated after transcription, has been reported in yeast (47,50,51). Other possibilities (*e.g.* high-affinity transporters upregulated at high nutrient levels) previously observed in diatoms for other nutrients like nitrate (52) might occur as well for phoshorus. The existence of transporters with different regulations and kinetics is in agreement with previous works that reported variations in K_{eff} for species like *Cosmarium abbreviatum* (21–23, but see also 19), and the identification of up to 24 putative P transporter genes (including mitochondrial carrier proteins) in *P. tricornutum* upregulated at different phosphorus conditions (28). More than two types of transporters may be present in the cell surface indeed (47), leading to a finer regulation of the P uptake and a greater capacity to exploit phosphate gradients. Our model provides a simplified version of this transporter diversity, in which transporter$_1$ and transporter$_2$ can represent clusters of P uptake proteins upregulated at different phosphorus levels.

The empirical V_{max} patterns and the model parameterization required to reproduce such patterns suggest differences in the cellular responses to phosphorus limitation and nutrient pulses. For example, the maximum synthesis rate for low-affinity transporters required to reproduce V_{max} peaks after P pulses was notably higher than that for high-affinity transporters to reproduce V_{max} increases at low P levels (unless $K_2 > 3.3$ µM was used). Analogously, we included different function types (*i.e.* step vs continuous) to describe the dynamics of both transporters (Eq. [5] and Eq. [7]). The expression of high-affinity

transporters occurs at low quotas (23), usually reached after a progressive nutrient depletion; cells with a finer control on the expression of these transporters would make a better use of their internal phosphorus resources and, therefore, would be positively selected. On the contrary, in the case of low-affinity transporters, which mainly take advantage of high environmental P concentrations, quick responses might be selected for instead: the cells that respond faster will store more nutrients before they are again depleted, with the efficient use of resources being secondary. Indeed, alternative mechanisms faster than transporter synthesis (e.g. activity regulation of existing uptake sites) have been described in yeast for low-affinity transporters (47,50). These ideas about the different velocities and type of responses to phosphorus limitation and pulses somewhat resemble the findings reported by Menge et al. (53), who theoretically predicted that cells showing slow and sensitive plastic responses (*i.e.* a tortoise-like strategy) prevail in stable environments, whereas cells with fast plastic responses (*i.e.* a hare-like strategy) prevail in environments showing a higher variability (below certain limits). Interestingly, our results highlight the possibility for the same cell to develop the two strategies, alternating between them thanks to the different regulation of the two types of transporters.

The theoretical model, by considering the temporal dimension and potential mechanisms of the acclimation process, enabled the integration of the snapshots provided by our empirical measurements in a moving picture and broad conceptual framework (30,31). In light of our simulations, run under the scenarios defined by our experimental design, the V_{max} and acclimation stage of phosphorus limited *P. tricornutum* cells can be predicted from environmental and intracellular phosphorus levels, which mainly reflect the present and past nutrient history of the cell, respectively (Fig. S10; refs. 14,54). We can indeed classify *P. tricornutum´*s uptake acclimation responses along these environmental and intracellular nutrient gradients in four scenarios that can occur sequentially (Fig. 4): 1) low environmental and intracellular phosphorus levels, 2) high environmental P concentration and low *Q*, 3) low environmental P concentration and high *Q*, and 4) high environmental and intracellular phosphorus levels (although we did not observe the latter case during our experiments). The scenarios with both environmental and intracellular phosphorus at high or low levels represent homeostasis (i.e. intracellular phosphorus levels matching environmental concentrations) and could lead to stationary dynamics if conditions are prolonged in time. On the contrary, the other two scenarios represent transient situations resulting from environmental nutrient fluctuations and the lag in the cellular physiology. The V_{max} trends and gene expression patterns observed in our experiments and replicated by our model can therefore be understood as a kind of succession of acclimation responses (Fig. 4; see below for a description of each acclimation stage). Along this succession, the lag in the cell response may lead to a mismatch between

gene expression and nutrient uptake traits, as it occurred during our experiments (e.g. P_{high} at 100 h after the P pulse) and it has been suggested for *Prochlorococcus* sp. (17).

The scenario of high environmental and low intracellular phosphorus levels was observed in P_{low} and P_{high} immediately after P pulses. It was characterized by an increase in V_{max} which, according to our model, occurred due to the upregulation of low-affinity transporters (Figs. 2 and 4). The positive relationship between V_{max}, nutrient transporters, and nutrient levels has been linked to a maximization of the phytoplankton capacity to exploit usually scarce resources (5). Nevertheless, to the best of our knowledge, our model is the first theoretical effort that mechanistically reproduces the increase in V_{max} under these conditions. The increase in Q led to the scenario of low environmental and medium-high intracellular phosphorus levels, which was observed in P_{high} after pulse depletion. Here, V_{max} reached minimum values due to the downregulation of the synthesis of both transporter types (Figs. 1a, 2a and 4). This suggests a cost for the synthesis of transporters and maybe a potential trade-off with other cell functions: cells invest in nutrient transporters only when it provides an increase in nutrient uptake or cell growth is strongly nutrient limited, otherwise cells invest their resources on growth or the uptake of other nutrients (53,55). Finally, growth caused the draw-down of environmental and intracellular phosphorus levels observed in P_{ref}, and P_{low} and P_{high} 100 h after P pulses. In this scenario we found an increase in V_{max} promoted by the upregulation of high-affinity transporters (Figs. 2 and 4). This V_{max} increase and transport upregulation has been reported in nutrient limited cultures and natural populations of phytoplankton (6,9,10,17,24,28). Such V_{max} responses can be limited by extreme cellular quota conditions occurring at homeostatic scenarios and systems in a stationary phase. V_{max} can decrease due to a negative feedback of the internal phosphorus pool on P uptake or the synthesis of transporters when Q is close to Q_{max} (12). Also, Krumhardt et al. (9) reported a marked decrease in V_{max} in phosphorus-starved (Q close to Q_{min}) cultures of *Prochlorococcus* sp., not observed for *P. tricornutum* in the present study.

It is plausible that a similar succession of acclimation responses occurs in natural phytoplankton populations experiencing some degree of phosphorus deficiency and environmental variability. Nonetheless, the succession we described could be restricted to those species and ecotypes with both high and low affinity transporters, as some acclimation strategies might be absent in organisms with just one transporter type. Species and ecotypes with both high and low affinity transporters would be encountered more often in environments showing high nutrient variations (25), as is the case in the coastal waters inhabited by *P. triconutum*. Indeed, Scanlan et al. (25), in an analysis of several strains of *Prochlorococcus* and *Synechococcus*, reported that the only strain with genes coding for potentially both

high and low affinity transporter proteins likely inhabited an estuarine environment, whereas the strains from oligotrophic and less variable waters lacked genes coding for low-affinity transporters.

Based on the comparison of the acclimation responses in the three P pulse treatments, we suggest that the acclimation succession experienced by a specific cell type would depend on the environment. The amplitude of the acclimation succession (*i.e.* the V_{max} range in the present context) would tend to decrease from ecosystems (and seasons) with marked temporal nutrient gradients to ecosystems with narrow gradients (Fig. 2; Fig. S10). In addition, the dominant (i.e. most frequent) acclimation stage would change between ecosystems. For example, higher V_{max} values and the expression of high-affinity transporters as in P_{ref} would dominate in oligotrophic ecosystems. In this regard, Lomas et al. (10) reported that picocyanobacteria in the Sargasso Sea usually show higher V_{max} values in summer (strong phosphorus limitation) than in winter. On the contrary, the expression of low-affinity transporters could dominate in eutrophic environments (56). Other factors like temperature and the availability of non-limiting nutrients might also affect acclimation responses; for instance, temperature may influence the synthesis of transporter proteins (57). As a result, the succession of acclimation responses occurring at the organismal level might influence the fitness of the cells, the community composition and, therefore, interact with the ecological succession occurring at the community level at wider temporal scales (4,58).

Final remarks

Although maybe intrinsic to the concept of acclimation, the idea of a temporal sequence of cellular responses might not have been stressed enough in the literature on nutrient uptake acclimation. We believe that understanding acclimation as a succession of responses along the nutrient spatiotemporal gradient offers a novel framework that may contribute to integrating the diverse responses developed by phytoplankton.

Future studies analyzing the dynamics along nutrient spatiotemporal gradients of the traits involved in nutrient uptake in different phytoplankton groups, as well as the expression of genes coding for nutrient transporters, are key to disentangling the diversity of responses and underlying regulation pathways. Sequenced species like *Synechococcus* sp., *Micromonas* sp. or *Emiliana huxleyi* are good candidates. Empirical results could inform mechanistic theoretical models similar to the one proposed here, which could be indeed modified to include alternative or additional regulation mechanisms and transporters, and accommodated to other nutrients or resources. These multidisciplinary studies would chart a way

This is the accepted version of the following article: *Cáceres C, Spatharis S, Kaiserli E, Smeti E, Flowers H, Bonachela JA. Temporal phosphate gradients reveal diverse acclimation responses in phytoplankton phosphate uptake. ISME J (in press). doi 10.1038/s41396-019-0473-1.*

forward to assess the ecological importance of acclimation and bridge the gap between cellular physiology, community ecology, and evolution.

Acknowledgements

We thank the members of the Marine Resource Modeling group at Strathclyde University, specially M.R. Heath and M. Choua, for their comments on the model and our preliminary results. We would also like to acknowledge K. Griffiths for her help with ^{33}P handling. M. W. Lomas kindly advised on the methodology for measuring P uptake. Suggestions and comments provided by James Grover and discussions with R. Anadón, F. G. Taboada, S. Romero-Romero and R. González-Gil are greatly appreciated. This research has been supported by the Marine Alliance for Science and Technology for Scotland (MASTS). C.C., S.S., and J.A.B. were supported by the Marine Alliance for Science and Technology for Scotland (MASTS) pooling initiative, funded by the Scottish Funding Council (HR09011) and contributing institutions. E.K. is grateful to the John Grieve Bequest and the Biotechnology and Biological Sciences Research Council (BBSRC) for the New Investigator Grant Award BB/M023079/1.

Funding

This research has been supported by the Marine Alliance for Science and Technology for Scotland (MASTS). C.C., S.S., and J.A.B. were supported by the Marine Alliance for Science and Technology for Scotland (MASTS) pooling initiative, funded by the Scottish Funding Council (HR09011) and contributing institutions. Gene expression experiments and analysis performed by E.K. were funded by the Biotechnology and Biological Sciences Research Council (BBSRC) (Grant Award BB/M023079/1).

Conflict of interest

The authors declare that they have no conflict of interest.

This is the accepted version of the following article: *Cáceres C, Spatharis S, Kaiserli E, Smeti E, Flowers H, Bonachela JA. Temporal phosphate gradients reveal diverse acclimation responses in phytoplankton phosphate uptake. ISME J (in press). doi 10.1038/s41396-019-0473-1.*

References

1. Falkowski PG, Barber RT, Smetacek V. Biogeochemical controls and feedbacks on ocean primary production. Science. 1998; **281**: 200–6.

2. Field CB, Behrenfeld MJ, Randerson JT, Falkowski P. Primary production of the biosphere: integrating terrestrial and oceanic components. Science. 1998; **281**: 237–40.

3. Reynolds CS. The ecology of phytoplankton. Cambridge Uni-versity Press; Cambridge, UK: 2006.

4. Reynolds C, Dokulil M, Padisák J. Understanding the assembly of phytoplankton in relation to the trophic spectrum: where are we now? Hydrobiologia. 2000; **424**: 147–52.

5. Caperon J, Meyer J. Nitrogen-limited growth of marine phyto-plankton—II. Uptake kinetics and their role in nutrient limitedgrowth of phytoplankton. Deep-Sea Res. 1972;19:619–32.

6. Gotham IJ, Rhee G-Y. Comparative kinetic studies of phosphate-limited growth and phosphate uptake in phytoplankton in continuous culture. J Phycol. 1981; **17**: 257–65.

7. Morel FMM. Kinetics of nutrient uptake and growth in phytoplankton. J Phycol. 1987; **23**: 137–50.

8. Zhang S-F, Yuan C-J, Chen Y, Chen X-H, Li D-X, Liu J-L, et al. Comparative transcriptomic analysis reveals novel insights into the adaptive response of *Skeletonema costatum* to changing ambient phosphorus. Front Microbiol. 2016; **7**: 1476.

9. Krumhardt KM, Callnan K, Roache-Johnson K, Swett T, Robinson D, Reistetter EN, et al. Effects of phosphorus starvation versus limitation on the marine cyanobacterium *Prochlorococcus* MED4 I: uptake physiology. Environ Microbiol. 2013; **15**: 2114–28.

10. Lomas MW, Bonachela JA, Levin SA, Martiny AC. Impact of ocean phytoplankton diversity on phosphate uptake. Proc Natl Acad Sci. 2014; **111**: 17540–5.

11. Sunda WG, Huntsman SA. Regulation of cellular manganese and manganese transport rates in the unicellular alga *Chlamydomonas*. Limnol Oceanogr. 1985; **30**: 71–80.

12. Riegman R, Stolte W, Noordeloos AAM, Slezak D. Nutrient uptake and alkaline phosphatase (EC 3: 1: 3: 1) activity of *Emiliania huxleyi* (Prymnesiophyceae) during growth under N and P limitation in continuous cultures. J Phycol. 2000; **36**: 87–96.

13. Michaelis L, Menten ML. Die kinetik der invertinwirkung. Biochem Z. 1913; **49**: 333–69.

14. Droop MR. Vitamin B 12 and marine ecology. IV. The kinetics of uptake, growth and inhibition in *Monochrysis lutheri*. J Mar Biol Assoc United Kingdom. 1968; **48**: 689–733.

15. Aksnes DL, Egge JK. A theoretical model for nutrient uptake in phytoplankton. Mar Ecol Prog Ser. 1991; **70**: 65–72.

16. Litchman E, Klausmeier CA. Trait-based community ecology of phytoplankton. Annu Rev Ecol Evol Syst. 2008; **39**: 615–39.

17. Reistetter EN, Krumhardt K, Callnan K, Roache-Johnson K, Saunders JK, Moore LR, et al. Effects of phosphorus starvation versus limitation on the marine cyanobacterium *Prochlorococcus* MED4 II: gene expression. Environ Microbiol. 2013; **15**: 2129–43.

18. Healey FP. Slope of the Monod equation as an indicator of advantage in nutrient competition. Microb Ecol. 1980; **5**: 281–6.

19. Fu F, Zhang Y, Bell PRF, Hutchins DA. Phosphate uptake and growth kinetics of *Trichodesmium* (Cyanobacteria) isolates from the North Atlantic Ocean and the Great Barrier Reef, Australia. J Phycol. 2005; **41**: 62–73.

20. Collos Y, Vaquer A, Souchu P. Acclimation of nitrate uptake by phytoplankton to high substrate levels. J Phycol. 2005; **41**: 466–78.

21. Rivkin RB, Swift E. Phosphate uptake by the oceanic dinoflagellate *Pyrocystis noctiluca*. J Phycol. 1982; **18**: 113–20.

22. Spijkerman E, Coesel PFM. Phosphorus uptake and growth kinetics of two planktonic desmid species. Eur J Phycol. 1996; **31**: 53–60.

23. Lin S, Litaker RW, Sunda WG. Phosphorus physiological ecology and molecular mechanisms in marine phytoplankton. J Phycol. 2016; **52**: 10–36.

24. Martiny AC, Coleman ML, Chisholm SW. Phosphate acquisition genes in *Prochlorococcus* ecotypes: evidence for genome-wide adaptation. Proc Natl Acad Sci. 2006; **103**: 12552–7.

25. Scanlan DJ, Ostrowski M, Mazard S, Dufresne A, Garczarek L, Hess WR, et al. Ecological genomics of marine picocyanobacteria. Microbiol Mol Biol Rev. 2009; **73**: 249–99.

26. Dyhrman ST, Jenkins BD, Rynearson TA, Saito MA, Mercier ML, Alexander H, et al. The

transcriptome and proteome of the diatom *Thalassiosira pseudonana* reveal a diverse phosphorus stress response. PLoS One 7 2012; e33768.

27. Liu Z, Koid AE, Terrado R, Campbell V, Caron DA, Heidelberg KB. Changes in gene expression of *Prymnesium parvum* induced by nitrogen and phosphorus limitation. Front Microbiol. 2015; **6**: 631.

28. Cruz de Carvalho MH, Sun H, Bowler C, Chua N. Noncoding and coding transcriptome responses of a marine diatom to phosphate fluctuations. New Phytol. 2016; **210**: 497–510.

29. Smith SL, Yamanaka Y, Pahlow M, Oschlies A. Optimal uptake kinetics: physiological acclimation explains the pattern of nitrate uptake by phytoplankton in the ocean. Mar Ecol Prog Ser. 2009; **384**: 1–12.

30. Dick GJ. Embracing the mantra of modellers and synthesizing omics, experiments and models. Environ Microbiol Rep. 2017; **9**: 18–20.

31. Bonachela JA, Raghib M, Levin SA. Dynamic model of flexible phytoplankton nutrient uptake. Proc Nat Acad Sci. 2011; **108**: 20633–8.

32. Button DK. Nutrient uptake by microorganisms according to kinetic parameters from theory as related to cytoarchitecture. Microbiol Mol Biol Rev. 1998; **62**: 636–45.

33. Mann KH, Lazier JRN. Dynamics of marine ecosystems:biological-physical interactions in the oceans. John Wiley & Sons;Oxford, UK; 2013.

34. Visser M, Batten S, Becker G, Bot P, Colijn F, Damm P, et al. Time series analysis of monthly mean data of temperature, salinity, nutrients, suspended matter, phyto-and zooplankton at eight locations on the Northwest European shelf. Dtsch Hydrogr Zeitschrift. 1996; **48**: 299–323.

35. Blauw AN, Beninca E, Laane RWPM, Greenwood N, Huisman J. Dancing with the tides: fluctuations of coastal phytoplankton orchestrated by different oscillatory modes of the tidal cycle. PLoS One 7. 2012; e49319.

36. Tovar-Sanchez A, Sañudo-Wilhelmy SA, Garcia-Vargas M, Weaver RS, Popels LC, Hutchins DA. A trace metal clean reagent to remove surface-bound iron from marine phytoplankton. Mar Chem. 2003; **82**: 91–9.

37. Siaut M, Heijde M, Mangogna M, Montsant A, Coesel S, Allen A, et al. Molecular toolbox for studying diatom biology in *Phaeodactylum tricornutum*. Gene. 2007; **406**: 23–35.

38. Vandesompele J, De Preter K, Pattyn F, Poppe B, Van Roy N, De Paepe A, et al. Accurate normalization of real-time quantitative RT-PCR data by geometric averaging of multiple internal control genes. Genome Biol. 2002; **3**: 0034.1-0034.12.

39. Kaiserli E, Paldi K, O'Donnell L, Batalov O, Pedmale U V, Nusinow DA, et al. Integration of light and photoperiodic signaling in transcriptional nuclear foci. Dev Cell. 2015; **35**: 311–21.

40. Quinn GP, Keough MJ. Experimental design and data analysis forbiologists. Cambridge University Press; Cambridge, UK; 2002.

41. R Core Team. 2017. R: A language and environment for statistical computing. R Foundation for Statistical Computing, Vienna, Austria. Available from http://www.R-project.org/

42. Pinheiro J, Bates D, DebRoy S, Sarkar D, Heisterkamp S, Van Willigen B, et al. Package "nlme." Linear nonlinear Mix Eff Model. 2017; R package version 3.1-131. URL https://CRAN.R-project.org/package=nlme

43. Lenth R. Emmeans: Estimated marginal means, aka least-squares means. 2018; R Package Version 1.3.0. URL https://CRAN.R-project.org/package=emmeans

44. Benjamini Y, Hochberg Y. Controlling the false discovery rate: a practical and powerful approach to multiple testing. J R Stat Soc Ser B. 1995; **57**: 289–300.

45. Molina Grima E, García Camacho F, Sanchéz Pérez JA, Fernández Sevilla JM, Acién Fernández FG, Contreras Gómez A. A mathematical model of microalgal growth in light-limited chemostat culture. J Chem Technol Biotechnol Int Res Process Environ Clean Technol. 1994; **61**: 167–73.

46. Olli K, Trunov K. Self-toxicity of *Prymnesium parvum* (Prymnesiophyceae). Phycologia. 2007; **46**: 109–12.

47. Secco D, Wang C, Shou H, Whelan J. Phosphate homeostasis in the yeast Saccharomyces cerevisiae, the key role of the SPX domain-containing proteins. FEBS Lett. 2012; **586**: 289–95.

48. Dyhrman ST. Nutrients and their acquisition: phosphorus phy-siology in microalgae. In: The physiology of microalgae. MABorowitzka, J Beardall, JA Raven, editors. Dordrecht, TheNetherlands. Springer; 2016. p. 155–83.

49. Feng T-Y, Yang Z-K, Zheng J-W, Xie Y, Li D-W, Murugan SB, et al. Examination of metabolic responses to phosphorus limitation via proteomic analyses in the marine diatom *Phaeodactylum tricornutum*.

Sci Rep. 2015; **5**:10373.

50. Hürlimann HC, Pinson B, Stadler-Waibel M, Zeeman SC, Freimoser FM. The SPX domain of the yeast low-affinity phosphate transporter Pho90 regulates transport activity. EMBO Rep. 2009; **10**: 1003–8.

51. Ghillebert R, Swinnen E, De Snijder P, Smets B, Winderickx J. Differential roles for the low-affinity phosphate transporters Pho87 and Pho90 in *Saccharomyces cerevisiae*. Biochem J. 2011; **434**: 243–51.

52. Song B, Ward BB. Molecular cloning and characterization of high-affinity nitrate transporter in marine phytoplankton. J Phycol. 2007; **43**: 542–52.

53. Menge DNL, Ballantyne F, Weitz JS. Dynamics of nutrient uptake strategies: lessons from the tortoise and the hare. Theor Ecol. 2011; **4**: 163–77.

54. Perry MJ. Phosphate utilization by an oceanic diatom in phosphorus-limited chemostat culture and in the oligotrophic waters of the central North Pacific. Limnol Oceanogr. 1976; **21**: 88–107.

55. Klausmeier CA, Litchman E, Levin SA. A model of flexible uptake of two essential resources. J Theor Biol. 2007; **246**: 278–89.

56. Zielinski BL, Allen AE, Carpenter EJ, Coles VJ, Crump BC, Doherty M, et al. Patterns of transcript abundance of eukaryotic biogeochemically-relevant genes in the Amazon River Plume. PLoS One 7. 2016; e0160929.

57. Toseland A, Daines SJ, Clark JR, Kirkham A, Strauss J, Uhlig C, et al. The impact of temperature on marine phytoplankton resource allocation and metabolism. Nat Clim Chang. 2013; **3**: 979-84.

58. Margalef R. Life-forms of phytoplankton as survival alternatives in an unstable environment. Oceanol acta. 1978; **1**: 493–509.

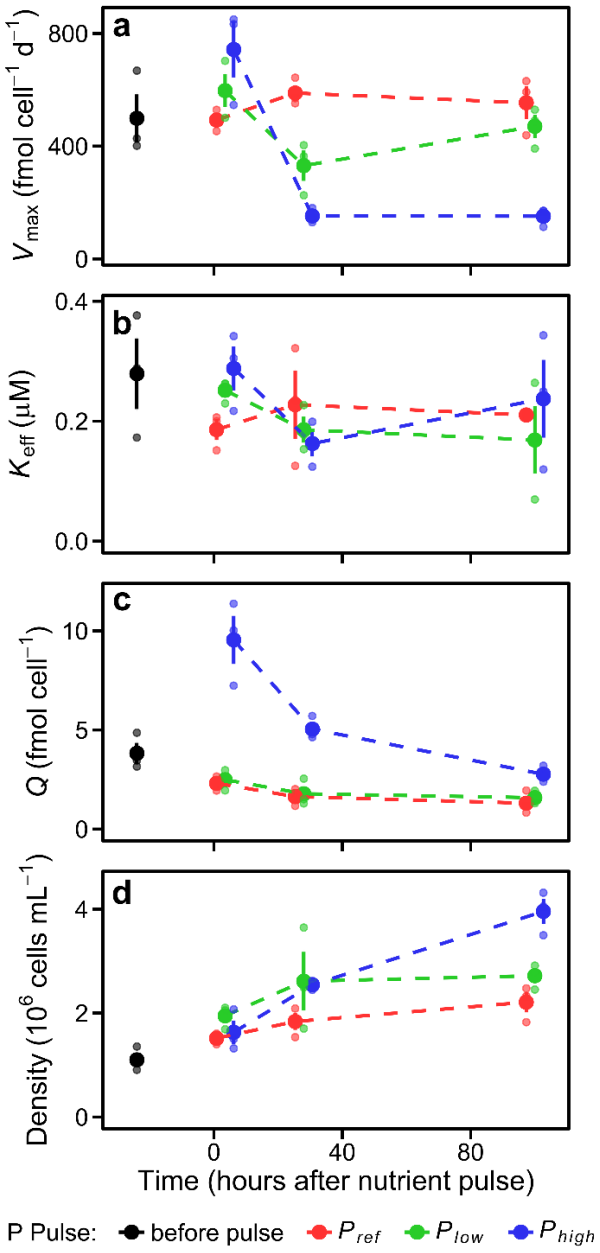

Fig. 1 Dynamics of the population and cellular traits measured in the different P pulse treatments. (a) Maximum phosphorus uptake rate (V_{max}). (b) Effective half saturation constant for phosphorus (K_{eff}). (c) Phosphorus quota. (d) Cell density. Big dots represent mean values. Small dots are the observations from the three experiments. Error bars show standard error estimated from untransformed data. Dashed lines join mean values. The horizontal position of the dots is slightly adjusted to avoid overlapping.

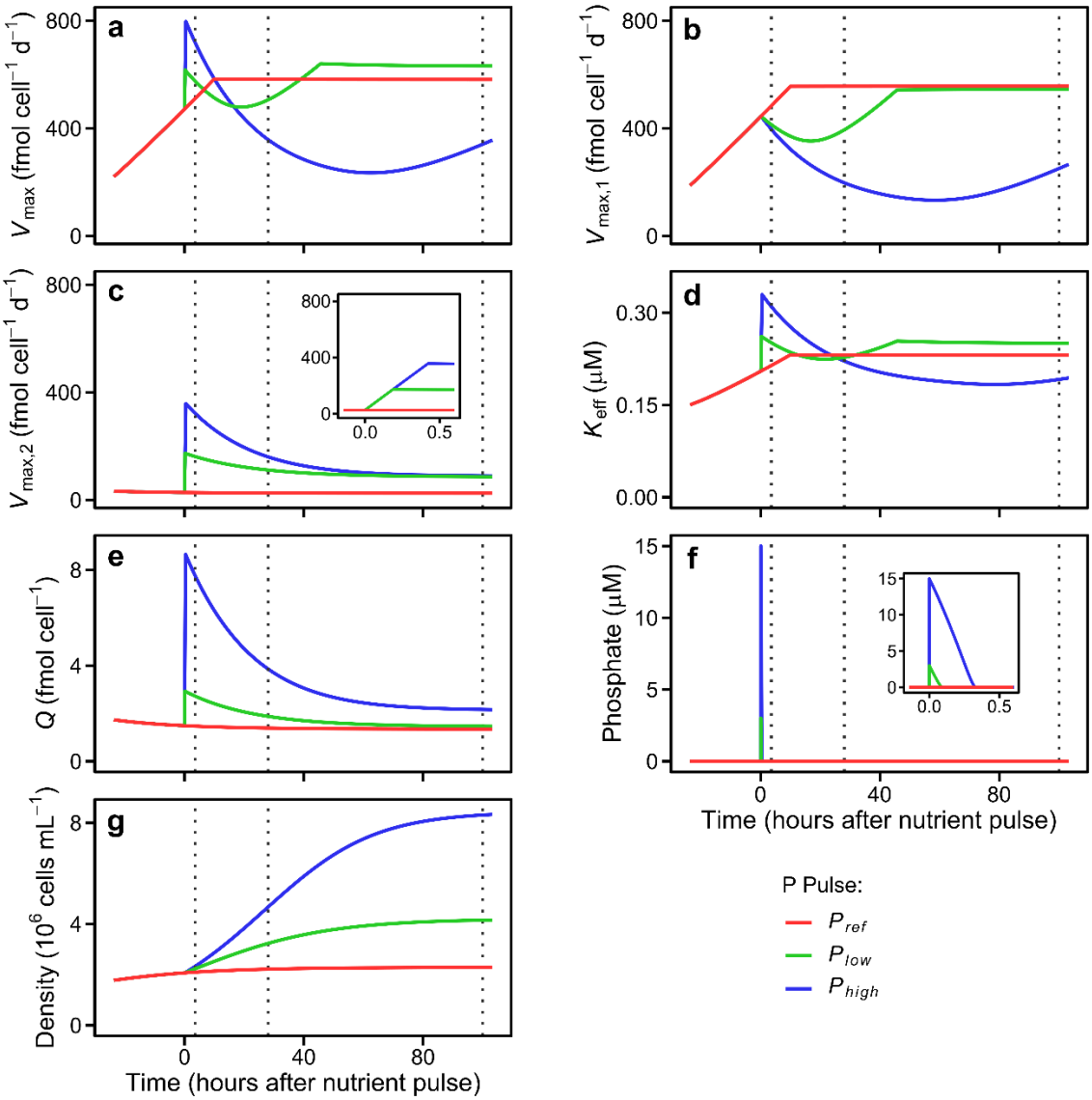

Fig. 2 Dynamics of cellular and population traits predicted by the model in nutrient regimes analogous to those occurring in cultures. (a) Maximum phosphorus uptake rate (V_{max}). (b) Maximum phosphorus uptake rate for transporter$_1$. (c) Maximum phosphorus uptake rate for transporter$_2$ ($V_{max,2}$); the inset shows a zoom of the $V_{max,2}$ just when the pulses occur (note the different x-axis scale). (d) Effective half saturation constant for phosphorus (K_{eff}). (e) Phosphorus quota. (f) Extracellular phosphate concentration; the inset shows a zoom when the pulses occur (note the different x-axis scale). (g) Cell density. To facilitate comparison with empirical results, vertical dotted lines indicate the times when measurements were taken during the experiments.

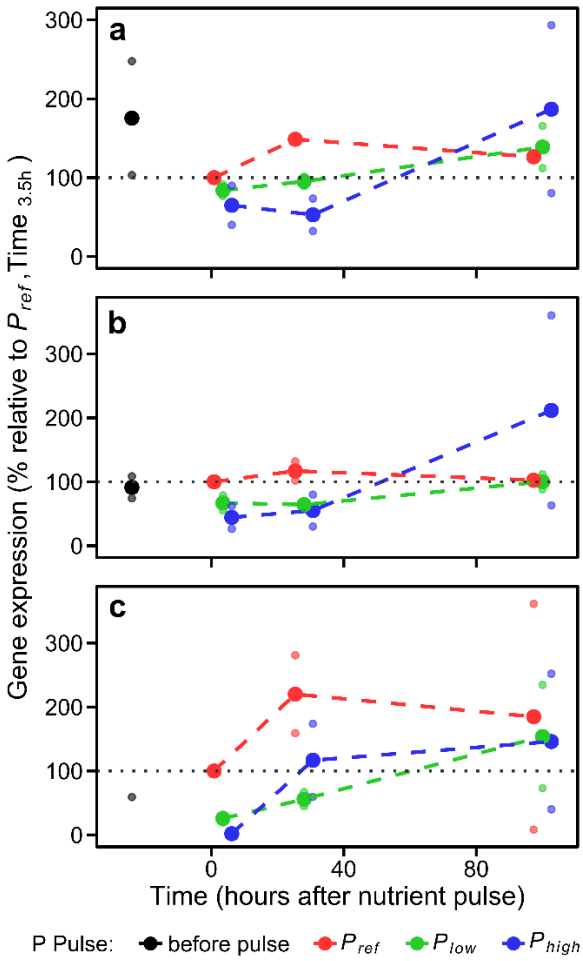

Fig. 3 Gene expression patterns in the different levels of phosphate addition. (a) *Na/Pi 47666*. (b) *Na/Pi 47667*. (c) *Pi 39515*. Big dots represent mean values. Small dots are the observations from experiments 2 and 3. Dashed lines join mean values. Grey dotted lines point out the reference level (i.e. 100%). The horizontal position of the dots is slightly adjusted to avoid overlapping.

This is the accepted version of the following article: *Cáceres C, Spatharis S, Kaiserli E, Smeti E, Flowers H, Bonachela JA. Temporal phosphate gradients reveal diverse acclimation responses in phytoplankton phosphate uptake. ISME J (in press). doi 10.1038/s41396-019-0473-1.*

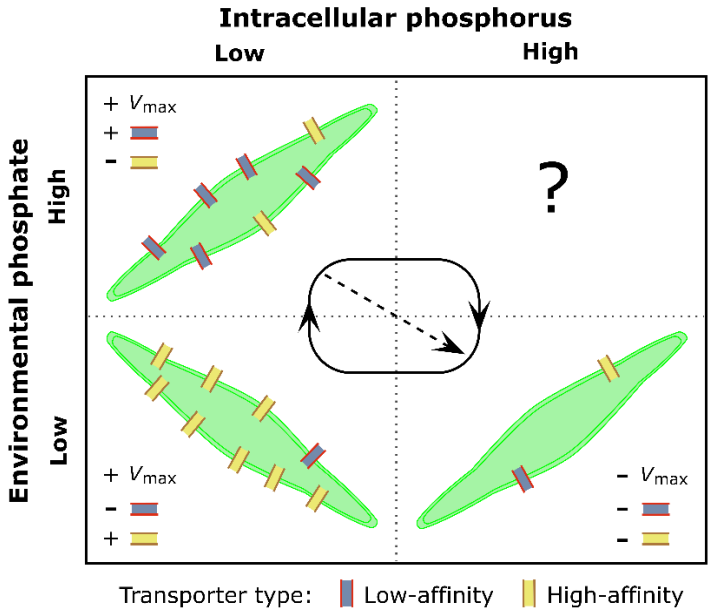

Fig. 4 Schematic figure representing the stages of phosphate uptake acclimation in *P. tricornutum* under different nutrient scenarios along the nutrient spatiotemporal gradient. Black arrows indicate the dominant direction of the acclimation succession. The dashed arrow shows the alternative acclimation succession pathway observed in our experiments. The + sign indicates an increase in trait value or transporter number, whereas – shows a decrease in trait value or transporter number.

Supplementary information

Phosphate uptake bioassays

Phosphate uptake bioassays consisted in a set of measurements of P uptake rate at different environmental P concentrations. These P uptake rate-environmental P pairs were subsequently employed to estimate the V_{max} and K_{eff} by fitting the Michaelis-Menten function:

$$V = V_{\max} \frac{P}{P + K_{\text{eff}}} \qquad [S1]$$

The culture aliquot was diluted for the uptake bioassays from cells counted using an inverted microscope and quick-read disposable chambers. We incubated treatments from 0.1 to 10 µM P in the first set of bioassays, but uptake rates at 10 µM P were excluded when fitting the uptake curves because their error was frequently higher and P uptake rate saturated at lower P levels. We incubated two additional vials with the same amount of cells and $H_3{}^{33}PO_4$ but a very high concentration of non-radioactive P (300 µM) to be used as blanks (the uptake of $H_3{}^{33}PO_4$ was negligible). The incubations were conducted in glass vials and finished after 20 min by adding 300 µM of H_3PO_4. We employed low incubation times to prevent the occurrence of changes in cell abundance and acclimation responses affecting V_{max} and K_{eff} during incubations. Samples were then gently filtered through 25 mm glass fiber filters of 0.7 µm of pore size. Filters were washed with a solution of oxalic acid to remove the ^{33}P attached to the cells (1,2). Filters were subsequently placed in scintillation vials, immersed in scintillation liquid, and kept in the dark for at least 12 h.

After measuring the radioactivity in the filters, the rate of P uptake rate (V, fmol cell^{-1} d^{-1}) was estimated using the following equation (3):

$$V = \left(R_f - R_b\right) \frac{P}{R_a \cdot T \cdot N}, \qquad [S2]$$

where R_f and R_b represent the radioactivity (corrected by the activity decay between the bioassay and measurement) in non-blank and blank filters, respectively (Table S1); P is the non-radioactive P concentration during the incubation (µM); R_a is the radioactivity added; T is the incubation time (d^{-1}); and N is the cell concentration (cell L^{-1}).

Intracellular phosphorus measurement

We digested the organic phosphorus contained in the filters by placing the filters in glass vials with 2 mL of concentrated (70%) nitric acid. Vials were fitted using a glass stopper as a cold finger cape and placed on a hotplate at a gentle boil for 1 hour. After they cooled, we added 10 mL of MilliQ water and we transferred it to a 100 mL volumetric flask. We rinsed the filters with three further 10 mL aliquots of MilliQ water. We then neutralized the solution by adding p-nitrophenol indicator (0.1% solution), 5 M NaOH, and 0.5 M sulphuric acid. Once the solution cooled, the flask was made up to volume. Proper blanks (filters washed with salt water and oxalate solution) were also prepared.

The intracellular phosphorus or quota (fmol cell^{-1}) was estimated from the inorganic phosphorus concentration measured in the digested solution (P_{ds}) according to the following equation:

$$Q = \frac{(P_{ds} - P_{ds\_blank})\, Vol_{flask}}{N \cdot Vol_f}, \qquad [S3]$$

where Vol_{flask} is the volume of the volumetric flask, N is the cell concentration in the culture analyzed, Vol_f is the volume of culture filtered, and P_{ds_blank} is the phosphorus concentration measured in the digested solution for the blank (Table S1).

Gene expression: RNA extraction and quantitative Real-Time PCR analysis (qRT-PCR)

Quantitative RT-PCR was performed using a StepOnePlus Real Time instrument (Thermofisher), Brilliant III UltraFast SYBR QPCR Master Mix (Agilent). Reactions were performed in four technical replicates on two biological replicates. The following cycling conditions were used for quantitative PCR: 2 min at 95°C, 50 cycles at 95°C for 3 s, and 59.5°C for 30 s. Melting curve analysis from 60 - 90°C was performed to monitor the specificity of the amplification. The quantitative real-time PCR procedure used follows the MIQE (Minimum Information for Publication of Quantitative Real-Time PCR Experiments) guidelines (4). The sample specific amplification efficiency was calculated according to the StepOne™ Software v2.2 (Life Technologies) using the slope of the regression line in the standard curve (standard dilution series: serial 4-fold dilutions, number of dilution points: 6). From this standard curve the software interpolated the target quantities of each gene, which was later used to calculate the relative fold differences.

Statistical analyses

We fitted the following mixed model to analyze the effects of P addition on the temporal dynamics of V_{max}, K_{eff}, V_{max}: K_{eff}, Q, and cell abundance:

$$y_{ijk} = mean + (P\ pulse)_i + (Time)_j + (P\ pulse\ x\ Time)_{ij} + (Experiment)_k + e_{ijk} \quad [S4]$$

where y_{ijk} is the value of the response variable at the level *i*, *j* and *k* of the factor *P pulse*, *Time* and *Experiment*, respectively. *mean* is the overall mean of the response variable. $P\ pulse_i$, $Time_j$ and $Experiment_k$ represent the effects of the level *i* of the factor *P pulse*, *j* of the factor *Time*, and *k* of the factor *Experiment*, respectively. $(P\ pulse\ x\ Time)_{ij}$ represents the effect of the interaction between the two fixed factors. e_{ijk} is the unexplained error associated with the observation at the level *i*, *j* and *k* of the factor *P pulse*, *Time*, and *Experiment*, respectively. *P pulse* had three levels, which correspond to the different P concentrations supplied to the cultures at day 6 of the experiment: P_{ref}, P_{low} and P_{high}. *Time* also had three levels, which are associated with the three time points of 3.5 h, 28 h and 100 h after the nutrient pulse when measurements were conducted. *Experiment* had three levels, corresponding to each of the three replicated experiments. By including experiment as a random factor we account for the potential dependency of residuals from observations coming from the same experiment. A total sample size of 27 observations were employed to fit the model.

Multiple pairwise comparisons were restricted to fixed main effects. Specifically, we focused on comparisons respect to the *P pulse* reference level (P_{ref}) and associated with the temporal sequence of the experiments (i.e. 3.5 h - 28 h, and 28 h - 100 h). We compared P_{ref} with P_{low} and P_{high} at each level of the factor *Time*, and *28 h* with *3.5 h* and *100 h* at each level of the factor *P pulse* (Table S3).

Model parameterization and initial conditions

Because the acclimation responses we focus on are expected to be generally found in phytoplankton, our model can be applied to any species Here, however, we based the parameterization on either the results empirically observed for *P. tricornutum* or the available literature.

The values μ_∞ = 1.0 d^{-1} and Q_{min} = 1.31 fmol $cell^{-1}$ were obtained from measurements conducted during our experiments; these values are in agreement with those reported for diatoms or phytoplankton species of similar sizes (5,6).

On the other hand, there is a lack of empirical information about the uptake kinetics for specific phytoplankton P transporters. K_1 = 0.085 µM was inferred from K_{eff} and V_{max} measured in P_{ref} by the end of the experiments, when cells were mainly expressing transporters similar to $transporter_1$. We based on the equation for the effective half saturation constant (7):

$$K_{\mathrm{eff},i} = K_i + \frac{V_{\max}}{4\pi D r_c}, \qquad [S5]$$

where D ($m^2\ s^{-1}$) is the diffusivity constant for phosphorus in water and r_c is the radius of the spherical cell. This expression considers the possible effect of a boundary layer formed around the cell at low environmental P levels due to diffusion limitation and phosphorus uptake (7,8). We assumed r_c= 2.5 µm from microscopic observations and the size information provided by the supplier of the cultures. K_2 = 0.45 µM was based on nonpublished K_{eff} and V_{max} data obtained from semicontinuous cultures.

The effective V_{max} measured in the uptake bioassays can be expressed as the sum of the V_{max} associated with every transporter:

$$V_{max} = \sum_{i=1}^{j} V_{\max,i} = \sum_{i=1}^{j} k_{\mathrm{cat},i}\, n_i\,, \qquad [S6]$$

where $k_{cat,i}$ (d^{-1}) is the catalytic rate of transporter *i.* (i.e. the rate of dissociation between the pair $transporter_i$-phosphate ion occurred in the cytoplasm) and it is calculated from

$$k_{\mathrm{cat},i} = K_i\, k_{1,i} \quad [S7]\ ; \text{and } k_{1,i} = 4Dr_{s,i} \quad [S8]$$

with $k_{1,i}$ the encounter rate between P and the transporter *i* in the extracellular environment, and $r_{s,i}$ the radius of transporter *i* (see ref. (7) for further details and references). We used v_1 = 2900 d^{-1} and v_2 = 32000 d^{-1} based on the values used by Bonachela et al. (7). We set r_s = 2.5 x 10^{-3} µm for the two transporters, which is within the range employed in previous studies (7,9). We set c_H= 0.51 %, $c_{F,a}$ = 1.6, $c_{F,b}$ = 5, and g_H= 10^{-9} for the *H* and *F* functions. This g_H term was included in a step function (*H*) with a range between 0 and 1 (Eq. [7]). An alternative and/or additional step function could include negative values to consider the activation-inhibition, in addition to changes in protein expression, of low-affinity transporters as previously observed in yeast (10–12).

Negative density-dependent effects on phytoplankton growth could be mediated, among other processes, by mutual shading and the release of chemical compounds with inhibitory or toxic effects (13–16). Instead of modelling explicitly light and the release of inhibitory compounds, for the sake of simplicity we represented phenomenologically these negative effects by including a generic density-dependent term (αN^2) in the equation for the cell growth rate (Eq. [1]), with α = 5.5 x 10^{-21} L^2 $cell^{-1}$. According to this formulation, the higher the cellular abundance the higher the negative interaction between cells mediated by cell shading or inhibitory compounds. This density-dependent term may lead to unrealistic negative growth rates when Q is close to Q_{min} and N is very high. This was not the case during our simulations, but it might occur if the model is run in other scenarios, for which other growth rate functions

may be more appropriate. Alternatively, the αN^2 could be excluded when adapting the model to other systems.

The qualitative patterns predicted by our model for V_{max}, K_{eff}, Q and N were robust to changes in the values assigned to parameters and coefficients. Nevertheless, to replicate quantitatively the magnitude of the responses and the relative performances of the P pulse treatments observed in the experiments some parameters (*e.g.* $c_{F,a}$, $r_{s,i}$, c_H) must be within specific ranges. For example, due to the competition between both types of transporters for the cell surface (Eqs. [5] and [7]), the predicted V_{max} peaks after P pulses were restricted when the threshold c_H related to the surface area occupied by transporters was set to low values. The effects of modifying a specific parameter can be counterbalanced by simultaneously modifying the value of other parameters (*e.g.* in the case of c_H, by modifying $r_{s,i}$), so that similar model outputs can be obtained with different parameterizations.

Finally, we set initial conditions aiming to mimic those of the experiments, which resulted in N = 5 x 10^7 cells L^{-1}, P = 3 µM, Q = 1.2 x Q_{min} fmol $cell^{-1}$, n_1 = 4500 transporters $cell^{-1}$, and n_2 = 50 transporters $cell^{-1}$. These initial Q, n_1 and n_2 values were chosen taking into account that our cultures were intentionally phosphorus starved; nonetheless the model output is robust to modifications of these initial values. Pulses of 0, 3 and 15 µM P were included at t = 6 d to replicate the experimental design.

References

1. Tovar-Sanchez A, Sañudo-Wilhelmy SA, Garcia-Vargas M, Weaver RS, Popels LC, Hutchins DA. A trace metal clean reagent to remove surface-bound iron from marine phytoplankton. Mar Chem. 2003; **82**: 91–9.

2. Lomas MW, Bonachela JA, Levin SA, Martiny AC. Impact of ocean phytoplankton diversity on phosphate uptake. Proc Natl Acad Sci. 2014; **111**: 17540–5.

3. Fu F, Zhang Y, Bell PRF, Hutchins DA. Phosphate uptake and growth kinetics of *Trichodesmium* (Cyanobacteria) isolates from the North Atlantic Ocean and the Great Barrier Reef, Australia. J Phycol. 2005; **41**: 62–73.

4. Bustin SA, Benes V, Garson JA, Hellemans J, Huggett J, Kubista M, et al. The MIQE guidelines: minimum information for publication of quantitative real-time PCR experiments. Clin Chem. 2009; **55**: 611–22.

5. Admiraal W, Werner D. Utilization of limiting concentrations of ortho-phosphate and production of extracellular organic phosphates in cultures of marine diatoms. J Plankton Res. 1983; **5**: 495–513.

6. Edwards KF, Thomas MK, Klausmeier CA, Litchman E. Allometric scaling and taxonomic variation in nutrient utilization traits and maximum growth rate of phytoplankton. Limnol Oceanogr. 2012; **57**: 554–66.

This is the accepted version of the following article: *Cáceres C, Spatharis S, Kaiserli E, Smeti E, Flowers H, Bonachela JA. Temporal phosphate gradients reveal diverse acclimation responses in phytoplankton phosphate uptake. ISME J (in press). doi 10.1038/s41396-019-0473-1.*

7. Bonachela JA, Raghib M, Levin SA. Dynamic model of flexible phytoplankton nutrient uptake. Proc Nat Acad Sci. 2011; **108**: 20633–38.

8. Pasciak WJ, Gavis J. Transport limitation of nutrient uptake in phytoplankton. Limnol Oceanogr. 1974; **19**: 881–8.

9. Aksnes DL, Egge JK. A theoretical model for nutrient uptake in phytoplankton. Mar Ecol Prog Ser. 1991; **70**: 65–72.

10. Secco D, Wang C, Shou H, Whelan J. Phosphate homeostasis in the yeast Saccharomyces cerevisiae, the key role of the SPX domain-containing proteins. FEBS Lett. 2012; **586**: 289–95.

11. Hürlimann HC, Pinson B, Stadler-Waibel M, Zeeman SC, Freimoser FM. The SPX domain of the yeast low-affinity phosphate transporter Pho90 regulates transport activity. EMBO Rep. 2009; **10**: 1003–8.

12. Ghillebert R, Swinnen E, De Snijder P, Smets B, Winderickx J. Differential roles for the low-affinity phosphate transporters Pho87 and Pho90 in *Saccharomyces cerevisiae*. Biochem J. 2011; **434**: 243–51.

13. Vardi A, Formiggini F, Casotti R, De Martino A, Ribalet F, Miralto A, et al. A stress surveillance system based on calcium and nitric oxide in marine diatoms. PLoS Biol. 2006; **4**: 411-419.

14. Molina Grima E, García Camacho F, Sanchéz Pérez JA, Fernández Sevilla JM, Acién Fernández FG, Contreras Gómez A. A mathematical model of microalgal growth in light-limited chemostat culture. J Chem Technol Biotechnol Int Res Process Environ Clean Technol. 1994; **61**: 167–73.

15. Olli K, Trunov K. Self-toxicity of *Prymnesium parvum* (Prymnesiophyceae). Phycologia. 2007; **46**: 109–12.

16. Casotti R, Mazza S, Brunet C, Vantrepotte V, Ianora A, Miralto A. Growth inhibition and toxicity of the diatom aldehyde 2-trans, 4-trans-decadienal on *Thalassiosira weissflogii* (Bacillariophyceae). J Phycol. 2005; **41**: 7–20.

This is the accepted version of the following article: *Cáceres C, Spatharis S, Kaiserli E, Smeti E, Flowers H, Bonachela JA. Temporal phosphate gradients reveal diverse acclimation responses in phytoplankton phosphate uptake. ISME J (in press). doi 10.1038/s41396-019-0473-1.*

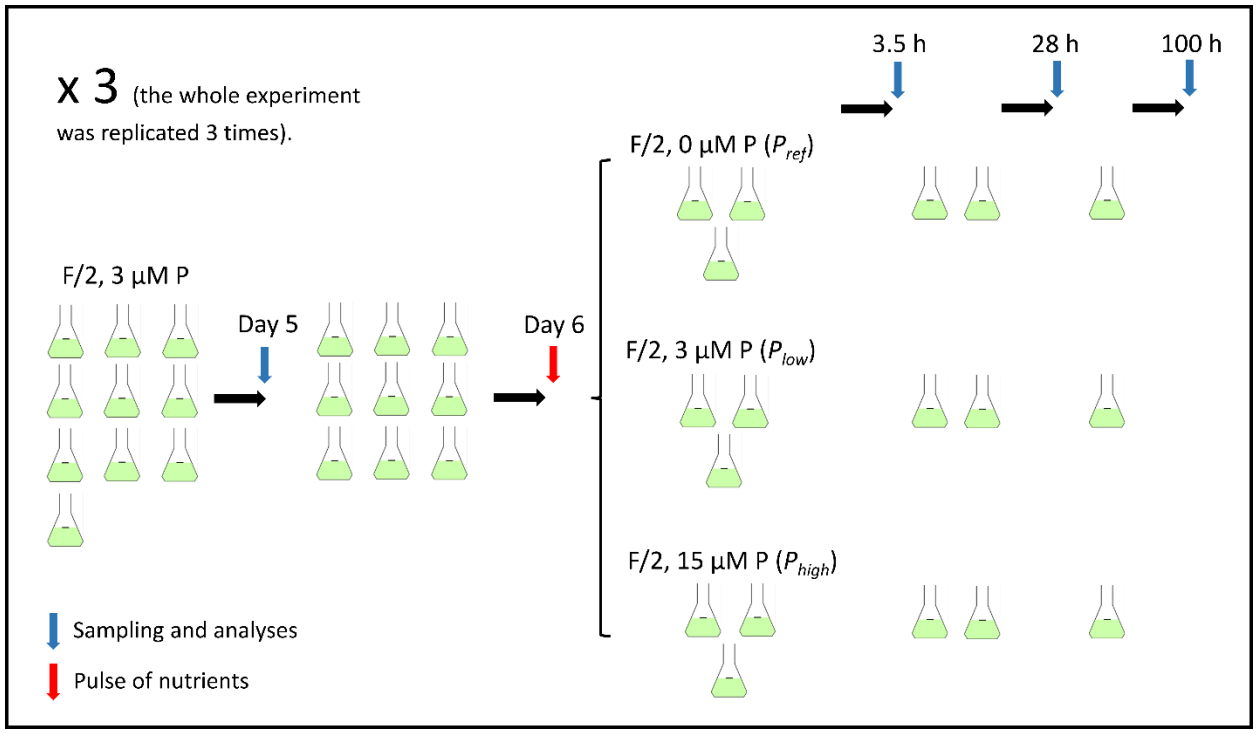

Fig. S1 Schematic figure representing the experimental design. Note that after P pulses the time is expressed in hours (h) after the P pulses. Maximum uptake rate and half saturation constant for phosphate uptake (both measured in bioassays), intracellular phosphorus content, and gene expression were measured at the times indicated by blue arrows

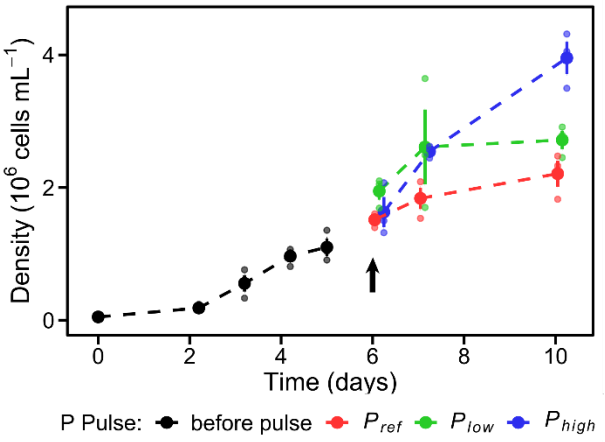

Fig. S2 Cell abundances along the experiments. Big dots indicate the mean from observations (small dots) obtained in the three experiments. Error bars indicate the standard error. The black arrow points out the time when nutrient pulses were added. The horizontal position of the dots is slightly adjusted to avoid overlapping.

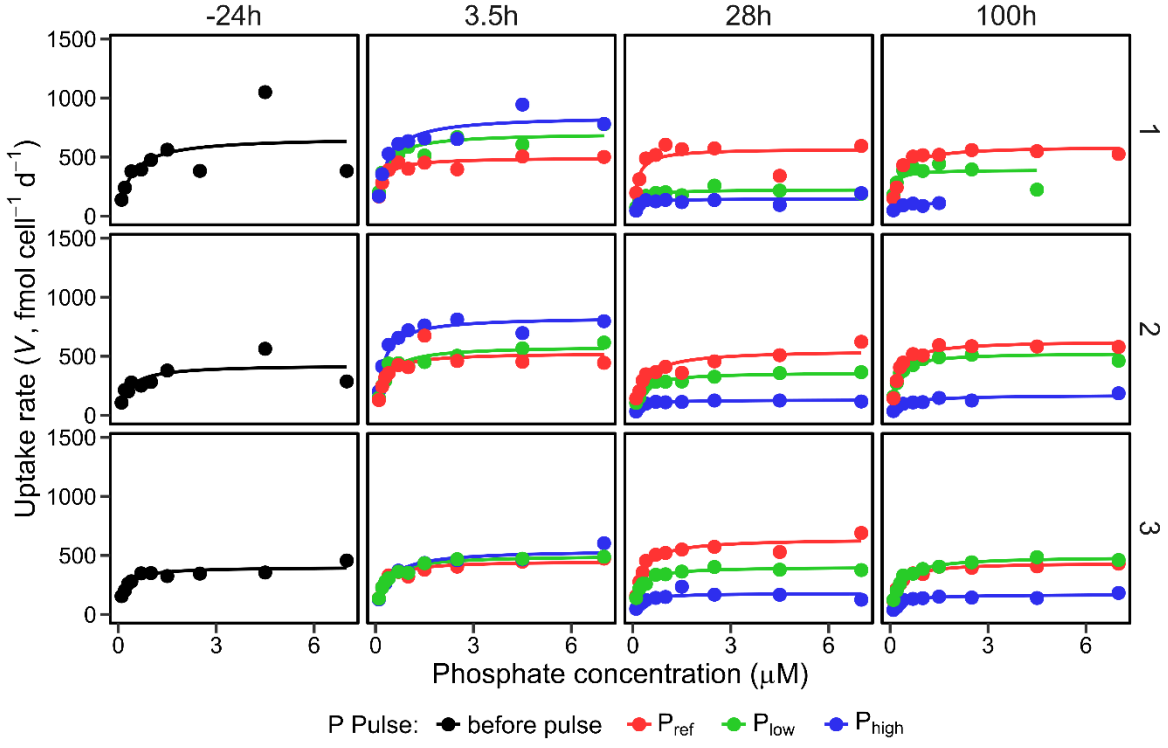

Fig. S3 Phosphate uptake rates and curves estimated from bioassays and the fitting of the Michaelis-Menten function. Numbers on the top of the panels indicate the time (hours) after the P pulse. Numbers on the right side of the panels point out the experiment replicate. Spurious negative uptake rates at 100 h in Experiment 1 were excluded from the analysis.

This is the accepted version of the following article: *Cáceres C, Spatharis S, Kaiserli E, Smeti E, Flowers H, Bonachela JA. Temporal phosphate gradients reveal diverse acclimation responses in phytoplankton phosphate uptake. ISME J (in press). doi 10.1038/s41396-019-0473-1.*

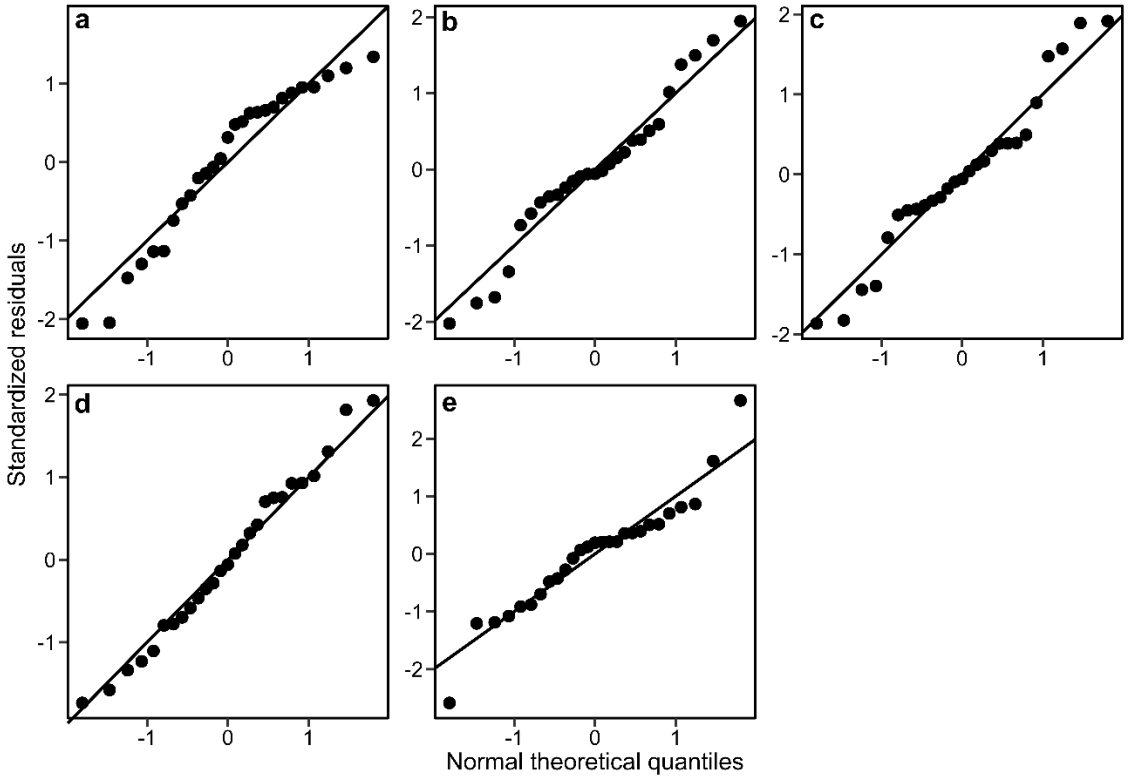

Fig. S4 Normal quantile-quantile plots of model residuals. (a) Maximum phosphate uptake rate (V_{max}), (b) effective half saturation constant for P uptake (K_{eff}), (c) V_{max}: K_{eff} ratio, (d) intracellular phosphorus, and (e) abundance.

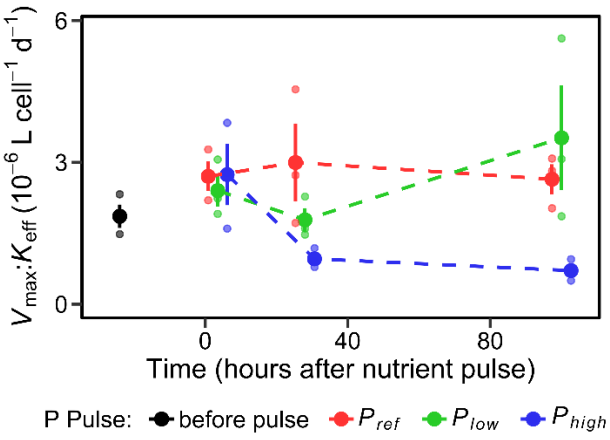

Fig. S5. Ratio between maximum phosphate uptake rate and effective half saturation constant (V_{max}: K_{eff}) obtained from empirical measurements. Big dots indicate the mean from observations (small dots)

obtained in the three experiments. Error bars indicate the standard error. The horizontal position of the dots is slightly adjusted to avoid overlapping.

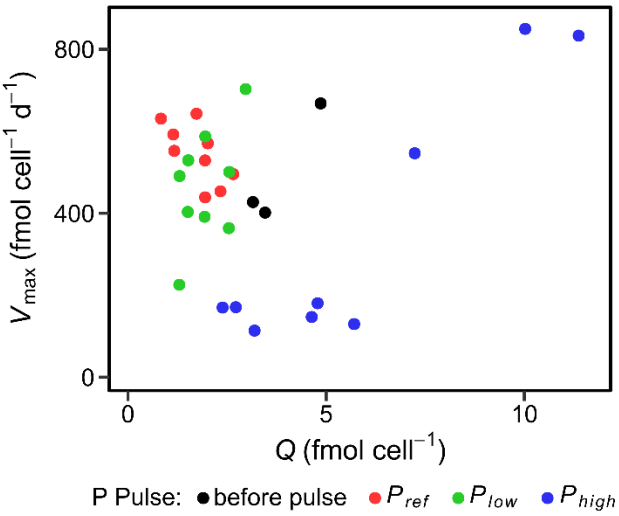

Fig. S6 Relationship between maximum phosphate uptake rate (V_{max}) and intracellular phosphorus (Q) from empirical measurements conducted for the different P pulse treatments.

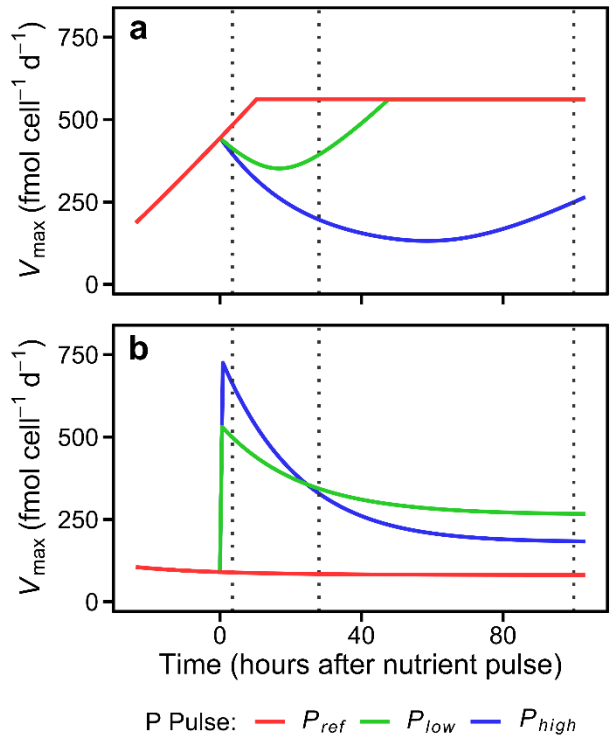

This is the accepted version of the following article: *Cáceres C, Spatharis S, Kaiserli E, Smeti E, Flowers H, Bonachela JA. Temporal phosphate gradients reveal diverse acclimation responses in phytoplankton phosphate uptake. ISME J (in press). doi 10.1038/s41396-019-0473-1.*

Fig. S7 Dynamics of maximum phosphate uptake rate (V_{max}) predicted by the model including just transporter$_1$ (a) or transporter$_2$ (b). Vertical dotted lines indicate the times when V_{max} was measured during the experiments.

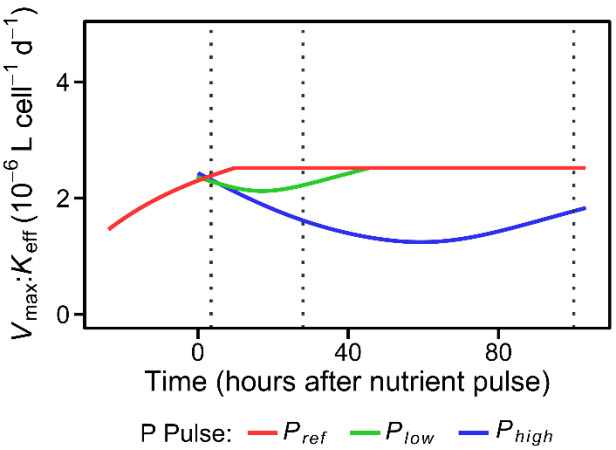

Fig. S8 Ratio between maximum phosphate uptake rate and effective half saturation constant (V_{max}: K_{eff}) predicted by our model for the three P pulse treatments.

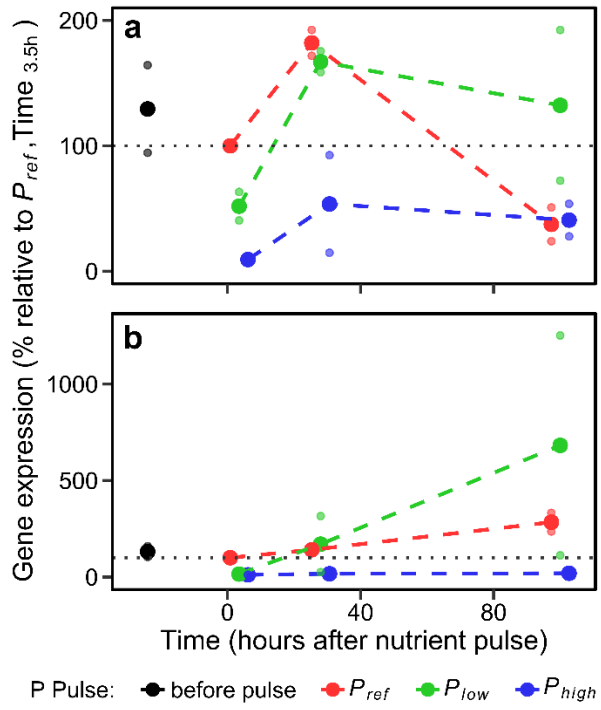

Fig. S9 Gene expression patterns in the different levels of P addition. (a) Alkaline phosphatase. (b) Carbamoyl phosphate synthetase. Big dots indicate the mean from observations (small dots) obtained in experiments 2 and 3. Grey dotted lines indicate the reference level (*i.e.* 100 %). The horizontal position of the dots is slightly adjusted to avoid overlapping.

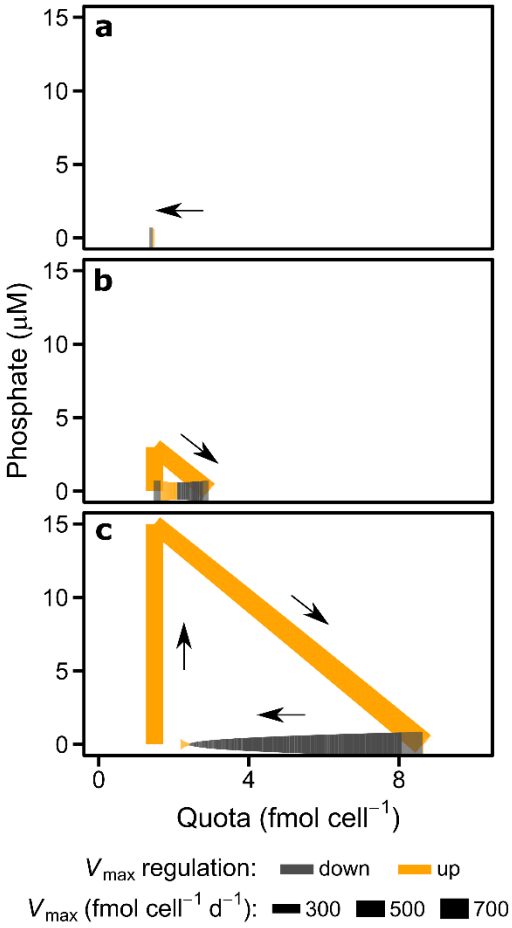

Fig. S10 Variation of maximum phosphorus uptake rate (V_{max}) along the phosphorus temporal gradient predicted by our model for P_{ref} (a) P_{low} (b) and P_{high} (c). The colours represent the sign of ($\frac{dV_{max}}{dt}$). Size scale indicates V_{max} values. Arrows indicate the direction of the temporal sequence.

This is the accepted version of the following article: *Cáceres C, Spatharis S, Kaiserli E, Smeti E, Flowers H, Bonachela JA. Temporal phosphate gradients reveal diverse acclimation responses in phytoplankton phosphate uptake. ISME J (in press). doi 10.1038/s41396-019-0473-1.*

Table S1. Symbols and values employed.

Symbol	Meaning	Units	Value/range
α	Density-dependent effect term	L^2 $cell^{-1}$	$5x10^{-21}$- $6x10^{-21}$
$A_{rel,i}$	Relative cell area occupied by transporters	-	-
c_H	Threshold for the maximum cell area occupied by transporters	-	0.50-0.54
$c_{F,a}$	Maximum quota proxy parameter	-	1.60
$c_{F,b}$	Shape parameter	-	2.5-7.5
D	Diffusivity constant for phosphorus in water	m^2 s^{-1}	$1.5x10^{-9}$
g_H	Threshold for the expression of transporter 2	-	10^{-1}- 10^{-10}
$k_{1,i}$	Encounter rate for transporter i	$(\mu mol/L)^{-1}$ x d^{-1}	-
$k_{cat,i}$	Catalytic rate of transporter i	d^{-1}	-
$K_{eff,i}$	Effective half saturation constant for transporter i	µM	-
K_1	Half saturation constant for transporter 1	µM	0.07-0.10
K_2	Half saturation constant for transporter 2	µM	0.4-0.5
n_i	Number of transporters of type i	transporters $cell^{-1}$	-
N	Cell concentration	cell L^{-1}	-
P_{ds}	Concentration of phosphorus in the digested solution	µM	-
P_{ds_blank}	Concentration of phosphorus in the digested solution for the blank	µM	-
Q	Phosphorus quota	fmol $cell^{-1}$	-
Q_{min}	Minimum cell quota	fmol $cell^{-1}$	1.31
R_a	Radioactivity added	µCi	0.20
R_b	Radioactivity (mean) in blank filters	µCi	-
R_f	Radioactivity in non-blank filters	µCi	-
r_{cell}	Cell radius	µm	2.50
$r_{s,i}$	Radius of transporter i	µm	0.0025
T	Incubation period	d	0.0139
μ	Growth rate	d^{-1}	-
μ_∞	Growth rate at infinite quota	d^{-1}	1.00
v_1	Maximum synthesis rate for transporter 1	sites $cell^{-1}$ d^{-1}	2600-3200
v_2	Maximum synthesis rate for transporter 2	sites $cell^{-1}$ d^{-1}	28000-36000
V	Phosphate uptake rate	fmol $cell^{-1}$ d^{-1}	-
V_{max}	Maximum phosphate uptake rate	fmol $cell^{-1}$ d^{-1}	-
$V_{max,i}$	Maximum phosphate uptake rate of i-type transporters	fmol $cell^{-1}$ d^{-1}	-
Vol_f	Volume of culture filtered	L	0.025
Vol_{flask}	Volume of the flask	L	0.10

This is the accepted version of the following article: *Cáceres C, Spatharis S, Kaiserli E, Smeti E, Flowers H, Bonachela JA. Temporal phosphate gradients reveal diverse acclimation responses in phytoplankton phosphate uptake. ISME J (in press). doi 10.1038/s41396-019-0473-1.*

Table S2. ANOVA results for the different variables analyzed. numDF: numerator degrees of freedom. denDF: denominator degrees of freedom. V_{max}: Maximum P uptake rate. K_{eff}: Effective half saturation constant for P uptake. V_{max}:K_{eff}: ratio between V_{max} and K_{eff}. *Q*: Intracellular phosphorus content. *N*: Phytoplankton abundance.

			V_{max}		K_{eff}		V_{max} : K_{eff}		*Q*		*N*	
Effect	numDF	denDF	F-value	p-value	F-value	p-value	F-value	p-value	F-value	p-value	F-value	p-value
P pulse	2	16	29.556	< 0.001	0.456	0.642	15.048	< 0.001	64.247	< 0.001	8.637	0.003
Time	2	16	29.906	< 0.001	2.091	0.156	3.918	0.041	25.191	< 0.001	20.303	< 0.001
P pulse x *Time*	4	16	20.696	< 0.001	2.005	0.142	5.848	0.004	4.078	0.018	2.718	0.067

Table S3. Pairwise comparisons for the different variables analyzed. V_{max}: Maximum P uptake rate. K_{eff}: Effective half saturation constant for P uptake. V_{max}:K_{eff}: ratio between V_{max} and K_{eff}. *Q*: Intracellular phosphorus content. *N*: Phytoplankton abundance.

			V_{max}		K_{eff}		V_{max} : K_{eff}		*Q*		*N*	
Time	P pulse	comparison	t-ratio	p-value	t-ratio	p-value	t-ratio	p-value	t-ratio	p-value	t-ratio	p-value
3.5h	-	P_{ref} - P_{low}	-1.281	0.320	-1.391	0.368	0.510	0.823	-0.345	0.755	-1.587	0.226
3.5h	-	P_{ref} - P_{high}	-2.809	0.025	-1.981	0.368	0.095	0.925	-8.237	< 0.001	-0.380	0.709
28h	-	P_{ref} - P_{low}	3.891	0.003	0.710	0.597	1.901	0.181	-0.318	0.755	-2.173	0.108
28h	-	P_{ref} - P_{high}	8.076	< 0.001	1.291	0.368	4.059	0.005	-5.875	< 0.001	-2.237	0.108
100h	-	P_{ref} - P_{low}	1.085	0.353	1.388	0.368	-0.948	0.536	-0.989	0.450	-1.474	0.240
100h	-	P_{ref} - P_{high}	7.661	< 0.001	-0.253	0.876	4.708	0.003	-3.658	0.006	-4.280	0.007
-	P_{ref}	3.5 - 28	-1.220	0.320	-0.694	0.597	-0.228	0.897	1.665	0.198	-1.192	0.301
-	P_{ref}	28 - 100	0.472	0.701	0.119	0.907	0.330	0.894	1.092	0.436	-1.220	0.301
-	P_{low}	3.5 - 28	3.952	0.003	1.407	0.368	1.163	0.524	1.691	0.198	-1.778	0.189
-	P_{low}	28 - 100	-2.333	0.057	0.797	0.597	-2.518	0.069	0.421	0.755	-0.520	0.665
-	P_{high}	3.5 - 28	9.665	< 0.001	2.578	0.243	3.736	0.007	4.027	0.004	-3.049	0.031
-	P_{high}	28 - 100	0.057	0.955	-1.426	0.368	0.979	0.536	3.309	0.011	-3.263	0.029

This is the accepted version of the following article: *Cáceres C, Spatharis S, Kaiserli E, Smeti E, Flowers H, Bonachela JA. Temporal phosphate gradients reveal diverse acclimation responses in phytoplankton phosphate uptake. ISME J (in press). doi 10.1038/s41396-019-0473-1.*